*Journal of Nepal Geological Society, 2011, Vol. 43 (Special Issue), pp. 307–314*

# Landslide susceptibility mapping in western Nepal using active fault map

***Hiroshi P. Sato[1] and Hiroshi Yagi[2]**

*[1]Geospatial Information Authority of Japan, Kitasato 1, Tsukuba 305-0811, Japan*
*[2]Yamagata University, 1-4-12, Kojirakawa, Yamagata 990-8560, Japan*
*(*Email: hsato@gsi.go.jp)*

## ABSTRACT

Eastern Nepal was struck by the Bihar-Nepal Earthquake (M8.2) in 1934; in western Nepal, however, no large earthquake has occurred since 1505, when an M8.5 earthquake occurred. The seismic gap in western Nepal is estimated to have a high potential for slip, and the severity of a huge earthquake that would rupture all or part of the gap has been reported. It is, therefore, of the utmost importance to prepare landslide susceptibility maps of western Nepal, whose hilly and mountainous terrain makes it prone to earthquake-induced landslides. In light of this, we have attempted to prepare a map of earthquake-induced landslide susceptibility for hill and mountain slopes in a 27 km by 27 km area of the Seti zone in western Nepal. We address only those landslides that occur on slopes angled five degrees and more. As basic data for the landslide inventory map preparation, we used the case of the 2005 Kashmir Earthquake (M7.6) in northern Pakistan, because no earthquake-induced landslide has occurred in the study area. As variables, we selected four factors: distance from the active fault, slope, convexity and pit-peak. For distance from the active fault, we used the fault map from a previous study. To calculate the other three factors, we used a 30-m-resolution digital elevation model. For the mapping we used the Information Value (InfoVal) method. The results gave four susceptibility classes of very low (landslide occurrence probability: 0 - 1%), low (1 - 4%), high (4 - 8%) and very high (8 - 70%).

**Keywords:** Landslide, earthquake, susceptibility, DEM, western Nepal

**Recieved:** 15 November 2010 **revision accepted:** 25 April 2011

## INTRODUCTION

Recent landslide inducing earthquakes include the 2004 Mid Niigata Prefecture Earthquake (M6.8) in Japan (Sato et al. 2005), the 2005 Kashmir (northern Pakistan) Earthquake (M7.6) (Sato et al. 2007), the 2008 Wenchuan (Great Sichuan) Earthquake (M7.9) in China (Sato and Harp 2009; Chigira et al. 2010; Qi et al. 2010) and the 2008 Iwate-Miyagi Nairiku Earthquake (M7.2) in Japan (Yagi et al. 2009). In eastern Nepal, the Bihar-Nepal Earthquake (M8.2) occurred in 1934; in western Nepal, however, no such a large earthquake has occurred since 1505 (M8.5) (e.g., Avouac et al. 2010). Earthquake-induced landslides cause serious disasters that threaten life, property and transportation networks. For effective measures against landslide disasters in western Nepal, an earthquake-induced landslide susceptibility map of that area is needed. Chacon et al. (2006) gave a general review of geographic information system (GIS) landslide mapping techniques and basic concepts of landslide mapping. According to Varnes (1984), landslide hazard mapping involves describing the probability of occurrence within a given period of time and a given area of this potentially damaging phenomenon. In contrast to landslide hazard mapping, landslide susceptibility mapping describes the spatial distribution of factors related to ground instability in order to determine landslide-prone zones without any prediction of when landslides might occur (Chacon et al. 2006). Chacon et al. (2006) also stated that this approach is useful for areas where it is difficult to secure enough information concerning the historical record of landslide events, meteorological records of rainfall and the magnitude/intensity of earthquakes that have triggered landslides.

For landslide susceptibility mapping, Varnes (1984) stated three basic principles: (1) The past and present are keys to the future, (2) the main conditions that cause landslides can be identified, and (3) degrees of hazard can be estimated. Chacon et al. (2006) added a fourth principle: (4) The risk associated with landslides may also be assessed and quantified.

Many researchers have proposed landslide susceptibility mapping in Nepal (e.g., Dhakal et al. 2000). However, the mapping of earthquake-induced landslide susceptibility has rarely been attempted in western Nepal (e.g., Regmi et al. 2010). This paper presents the methods and results of landslide susceptibility mapping in a large earthquake-prone area using the map of active faults. We address only those landslides at slopes of at least five degrees in angle.

## STUDY AREA

The study area is 27 km by 27 km in the Seti zone of western Nepal. The center of the study area is at 29°0′N latitude by 80°40′E longitude. Two active faults, the Main Boundary Fault (MBF) and the Himalayan Frontal Fault (HFF) (Kumahara and Nakata 2005), run through central

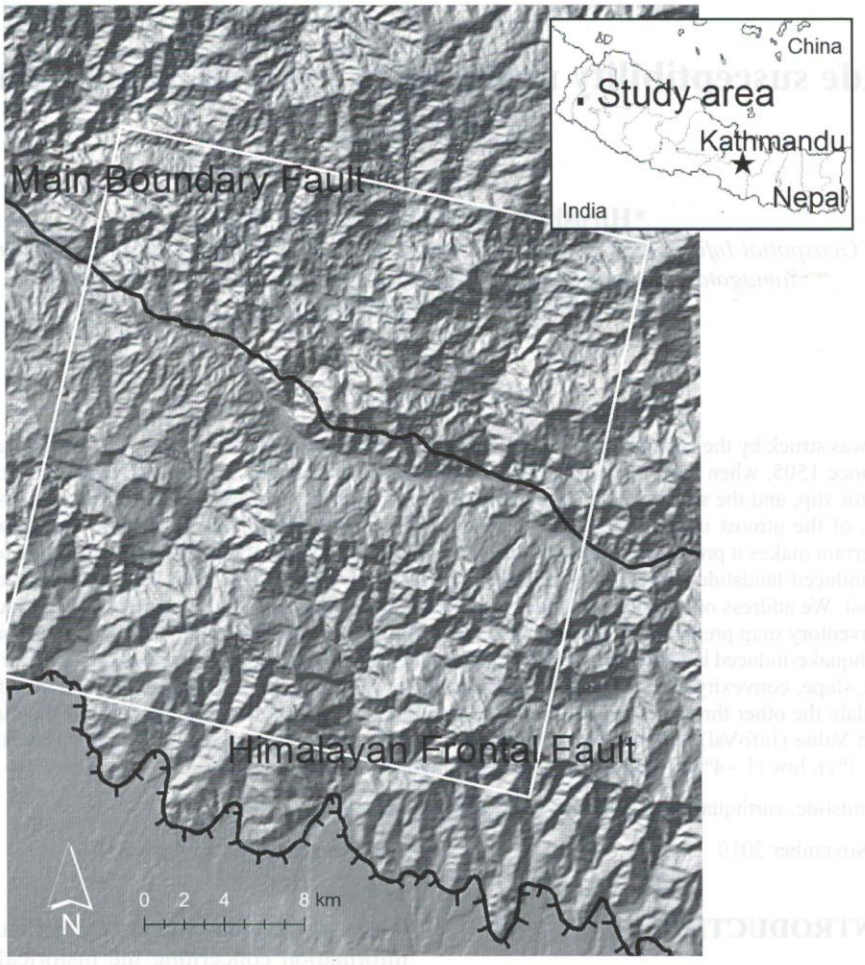


**Fig. 1: Location of study area**

and southern parts of the study area (Fig. 1). Geologically, the study area consists, from north to south, mainly of Precambrian-Paleozoic metamorphosed sandstone and quartzite (Mahabharat Mountains, elev. 1,000 - 2,500 m), the MBF, Miocene unconsolidated-weak consolidated fluvial deposits of the Siwalik formation (Churia Range, elev. 200 - 700 m), the HFF, and Holocene fluvial deposits in Terai (North Gangetic Plain) (Upreti 1999).

## METHOD

For the preparation of an earthquake-induced landslide susceptibility map for hill and mountain slopes, we started by collecting landslide inventory maps as the basic data, then we selected four causative factors (slope, convexity, pit-peak and distance from active faults) as the variables. Then, using the Information Value (InfoVal) method (Van Western 1997), we mapped 30-m-resolution grid-cell-based earthquake-induced landslide susceptibility, which corresponds to a map scale of 1/25,000. The reason for choosing this resolution will be explained below. A rough flowchart of the mapping method is shown in Fig. 2.

### Collection of landslide inventory as the basic data

As shown in Saha et al. (2005), basic data for landslide inventory is usually collected in the study area. In our case, however, instead of collecting it in the study area, we used basic data collected for northern Pakistan, where a strong earthquake occurred in 2005. There are three reasons for this.

First, no major earthquake has recently occurred in the study area, so if a landslide inventory was prepared by interpreting aerial photograph or satellite imagery, it would contain landslides triggered not only by the older earthquakes but also by heavy rains. Second, the 2005 Kashmir Earthquake showed a shallow rupture with a reverse fault-type focal mechanism, which represents the relative consumption between the Indian and Eurasian plates (Seno 2005). This tectonic situation also prevails in the study area (Bilham et al. 1997). Third, the Balakot-Garhi Fault (Kumahara and Nakata 2006) that triggered the 2005 Kashmir Earthquake runs parallel to the Main Boundary Thrust (MBT). Kumahara and Nakata (2005) also identified an active fault running parallel to the MBT in the study area (Fig. 1). Thus, the active fault distribution in northern Pakistan is similar to that in the study area.

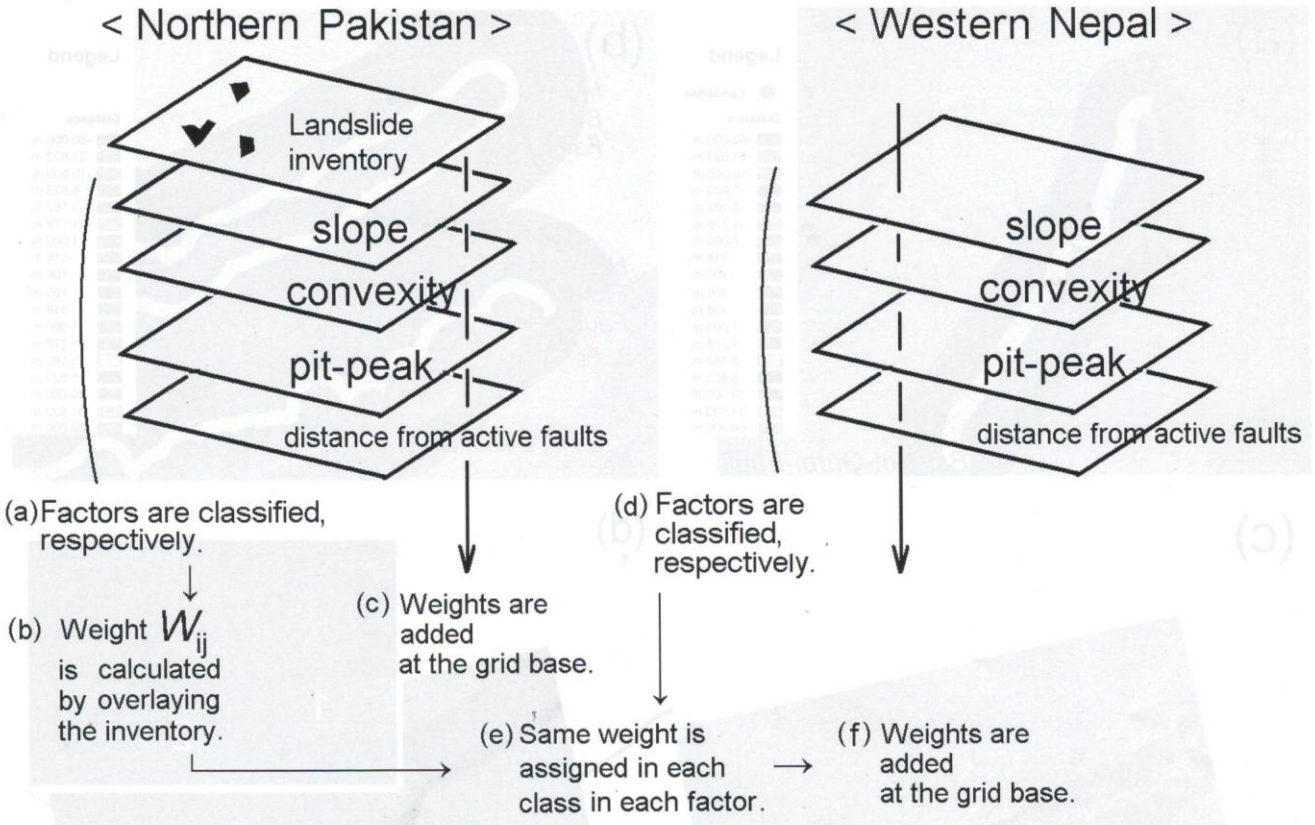


**Fig. 2: Flowchart of methodology for earthquake-induced landslide susceptibility mapping**

Since we selected a mapping resolution of 30 m, we chose landslides of at least 30 m × 30 m. This gave us 1,687 landslide sites (mostly shallow disrupted landslides) as basic data from the 2,424 landslides in the inventory (Sato et al. 2007). The resulting susceptibility map addresses the occurrence probability for landslides of this size.

**Selection of the four causative factors**

As shown in Fig. 2, the same four causative factors (slope, convexity, pit-peak and distance from active faults) were measured for northern Pakistan and the study area. We did not select geological unit as causative factor, for two reasons. First, in the case of the 2008 Wenchuan (Great Sichuan) Earthquake (M7.9) in China, no obvious correlation has been found between landslide concentration and geological unit (Qi et al. 2010). Second, geologic units written on geologic maps are not compatible between the two areas at 1/25,000 scale.

*Slope*

Slope angle was calculated from a digital elevation model (DEM) that is a 30-m-resolution global digital elevation map (GDEM). In calculating slope angle, we used a 3 × 3 moving window.

GDEMs were prepared by the Ministry of Industry, Trade and Information of Japan (MITI) and the National Aeronautics and Space Agency of the United States (NASA); a data download service is available on the Web (http://www.ersdac.or.jp). The GDEMs were produced by a photogrammetric method using TERRA/ASTER (Advanced Spaceborne Thermal Emission and Reflection Radiometer) stereo-viewed images. The shade map in Fig. 1 was produced from the GDEM.

*Convexity and pit-peak*

The calculation method for convexity and pit-peak is based on Iwahashi and Pike (2007). These two factors are thought to be related to the seismic wave. Iwahashi et al. (2010) investigated the correlation between Vs30 (the average velocity of an s-seismic wave from the surface to 30 m in depth) and convexity. They concluded that convexity correlates closely with Vs30. Furthermore, they investigated the correlation between Vs30 and pit-peak, and they also concluded that pit-peak correlates closely with Vs30.

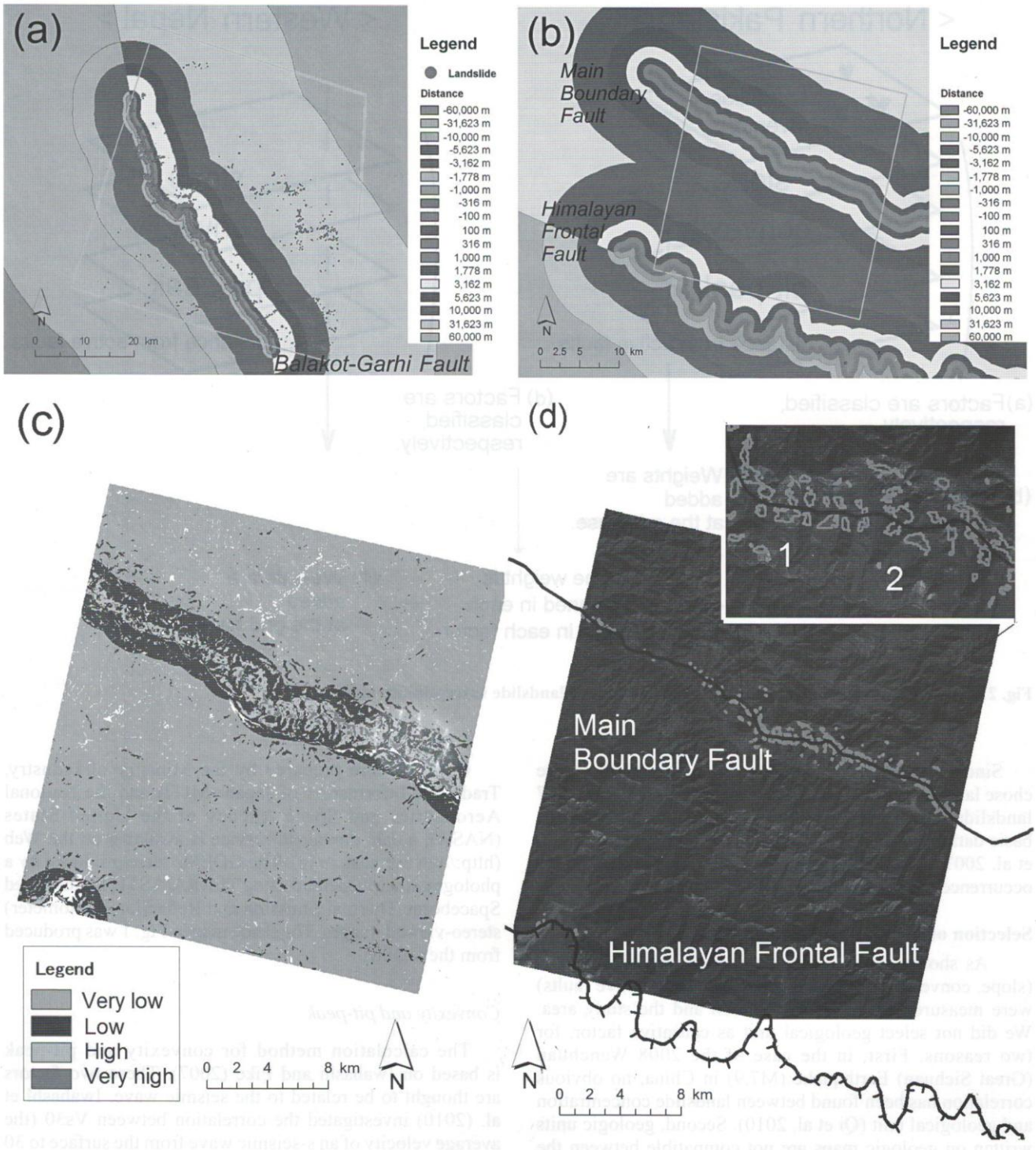


**Fig. 3: Distances from active faults, and the results of landslide susceptibility mapping, (a) Distance from the Balakot-Garhi Fault (Kumahara and Nakata 2005) in northern Pakistan. The 2,424 landslides overlain on the distance from the active fault were triggered by the 2005 Kahmir Earthquake (Sato et al. 2007). (b) Distances from the Main Boundary Fault and the Himalayan Frontal Fault. (c) The landslide susceptibility map produced for western Nepal (the study area), with same threshold as in Fig. 4 (northern Pakistan), was applied to the cumulative weights in western Nepal, then the susceptibility was divided into four classes. (d) An overlay of the 'very high' class shown in (c) on the Cartosat-1 satellite image.**

(a) Calculation of convexity

Surface curvature is measured by the 3 × 3 Laplacian filter, an image-processing operation that is used in edge enhancement, which yields positive values for convex-upward areas, negative values for concave areas, and zero for planar slopes (Iwahashi and Pike 2007). The convexity at each grid cell was defined as the number of convex-upward grid cells within a circle whose constant radius is ten grid cells (the circle occupies 314 grid cells) (Iwahashi and Kamiya 1995). The greater the convexity, the greater the magnitude of convexity. We calculated the convexity ratio by dividing convexity (number of convex-upward grid cells) by the 314 cells in each grid cell (northern Pakistan and western Nepal, the study area).

(b) Calculation of pit-peak

Pit-peak is used to express surface roughness (fine vs. coarse). It is calculated by extracting grid cells that outline the distribution of valleys and ridges in GDEM. These grid cells are identified from differences between the original GDEM and the GDEM derived by passing the original through the 3 × 3 median filter, i.e., the filter that was originally used to remove high-frequency spatial "noise" from a digital scene by replacing original values with values of central tendency (Iwahashi and Pike 2007). After the original GDEM is filtered, the obtained GDEM shows a smooth surface that is less rugged than the original relief. The difference between the two kinds of GDEM shows grid cells of "pit" (coincident with valley) and "peak" (coincident with ridge).

Iwahashi and Kamiya (1995) defined pit-peak at each grid cell as the cumulative number of pits and peaks within a circle whose constant radius is ten grid cells (the circle occupies 314 cells). The greater the pit-peak, the finer the land surface is. We calculated pit-peak ratio by dividing pit-peak by the 314 cells in each grid cell (northern Pakistan and western Nepal, the study area).

*Distance from an active fault*

Sato et al. (2007) reported that landslides triggered by the 2005 Kashmir Earthquake concentrated more at hanging walls than at foot walls. Furthermore, they reported that at least half of the landslides at hanging walls occurred within 2 km from the Balakot-Garhi Fault (Kumahara and Nakata, 2006); the rest of the landslides became less densely distributed with increasing distance from the fault. Chigira et al. (2010) also showed a similar tendency for the landslides triggered by the 2008 Wenchuan Earthquake.

For the Balakot-Garhi Fault in northern Pakistan, the distance from the fault was measured separately for the hanging wall side and for the foot wall side. In the study area, the HFF was conceptually split at the border between hanging wall and foot wall, which is a reverse fault (Kumahara and Nakata 2005). They also describe the MBF in the study area as a reverse fault. However, the MBF shows recent normal displacement along most of its length (Mugnier et al. 1994). Furthermore, for the entire Nepalese Himalaya, Kumahara and Nakata (2005) reported that the MBF shows as a right-lateral strike deformation in some sections. Therefore, to measure the distance from an active fault we do not conceptually split it at hanging walls and foot walls there.

## THE INFOVAL METHOD

Kamp et al. (2008) produced a landslide susceptibility map (four classes: very high, high, moderate and low) for northern Pakistan using the Analytical Hierarchy Process (Yagi 2003; Yoshimatsu and Abe 2006). However, this required expert opinions, and experts do not always share the same opinion. Therefore, in this study we mapped susceptibility by using the InfoVal method (Van Western 1997), a quantitative grid-cell-based method. This method has been used in landslide susceptibility mapping for northern Spain (Saha et al. 2005).

### Data preprocessing

In this method causative factors are classified to calculate weight; for data preprocessing, we used the same classes to classify the causative factors for northern Pakistan and western Nepal (Figs. 2a and 2d). Therefore, each class of each causative factor is uniquely compatible between the two areas. Slope data were divided into 36 classes (interval: 2°). Convexity and pit-peak ratio were respectively divided into 20 classes (interval: 0.05).

As shown in Figs. 3a and 3b, the distance from active faults was also classified as class thresholds of common logarithm 2, 2.5, 3, 3.25, 3.5, 3.75, 4, 4.5, and 4.8 (e.g., the original distance is 0 – 100 m, 100 – 316 m, 316 - 1,000 m, 1,000 - 1,778 m, 1,778 - 3,162 m, 3,162 - 5,623 m, 5,623 - 10,000 m, 10,000 - 31,623 m, 31,623 - 60,000 m). The reason we used common logarithm is that landslide concentration declined sharply with increasing distance from the active fault. Measuring the distance from the fault at a constant interval would not properly capture the distribution: Areas near the fault would lack definition, and areas far from the fault would have many classes with landslide concentrations approaching zero. Note that the distance is written as having a positive value for the hanging wall side and a negative value for the foot wall side. Finally, the distance was divided into 18 classes, respectively, for northern Pakistan and the study area.

### Weight calculation for northern Pakistan

In this method, the probability of landslide occurrence is considered in each class of each causative factor. As shown in Fig. 2b, the weight is calculated using Equation (1).

**Table 1: Weight ranges for the two areas**

| Causative factors | Northern Pakistan | Western Nepal (study area) |
|---|---|---|
| Slope | −1.93 - 1.18 | −1.93 - 1.18 |
| Convexity | −3.29 - 0.30 | −3.29 - 0.30 |
| Pit-peak | −1.53 - 0.18 | −1.53 - 0.18 |
| Distance | −6.07 - 2.76 | −0.93 - 2.76 |
| (Cummulative weight) | −10.82 - 4.18 | −6.15 - 4.21 |

$$W_{ij} = \log_e \left[ \frac{\left\{ \frac{(n_A)_{ij}}{(n_B)_{ij}} \right\}}{\frac{\sum_j (n_A)_{ij}}{\sum_j (n_B)_{ij}}} \right] \quad \text{.....(1)}$$

Where, $(n_A)_{ij}$ is the number of grid cells that contain landslides (landslide cells), in a certain class of a certain factor (equation 1); $(n_B)_{ij}$ is the total number of grid cells in a certain class of a certain factor. Therefore, $(n_A)_{ij}/(n_B)_{ij}$ (equation 1) is the landslide occurrence probability in a certain class of a certain factor. If $(n_A)_{ij}$ equals zero, then $W_{ij}$ cannot be calculated; however, such cases mostly occurred within the area less than five degrees in slope angle, so we did not map the susceptibility in such areas. In Equation (1), denominator of the anti-logarithm is the landslide occurrence probability for a certain factor. Therefore, the anti-logarithm in Equation (1) shows the normalized landslide occurrence probability for a certain factor 'i' and a certain class 'j' of that factor. The natural logarithm is used to address the large variation in weights (Van Western 1997). The higher $W_{ij}$ is, the higher the landslide susceptibility is. The middle column in Table 1 shows the weight range for each factor in northern Pakistan.

Next, as shown in Fig. 2c, weights for northern Pakistan are added at grid-cell base using Equation (2).

$$W = \sum_i \sum_j \delta_{ij} W_{ij} \quad \text{.....(2)}$$

Where, if a sample grid cell belongs to j-th class of a certain factor 'i', then $ä_{ij}$ equals 1 and otherwise it equals 0. After the calculation, cumulative weight was given to each grid cell, and the result yielded a maximum of 4.18 and a minimum of -10.82 (middle column of Table 1).

## Weight assignment for western Nepal

As no earthquake-induced landslide inventory is available in the study area, we cannot use Equation (1) to calculate the weight directly for the study area (western Nepal). However, classes correspond to each other between north Pakistan and the study area, as shown in Fig. 2e, so we assigns the obtained weight in each class for northern Pakistan to the corresponding class for the study area. After the assignment, as shown in Fig. 2f cumulative weight is given to each grid cell in the same manner for northern Pakistan. The result of the cumulative weight yields a maximum of 4.21 and a minimum of -6.15 (the right column of Table 1).

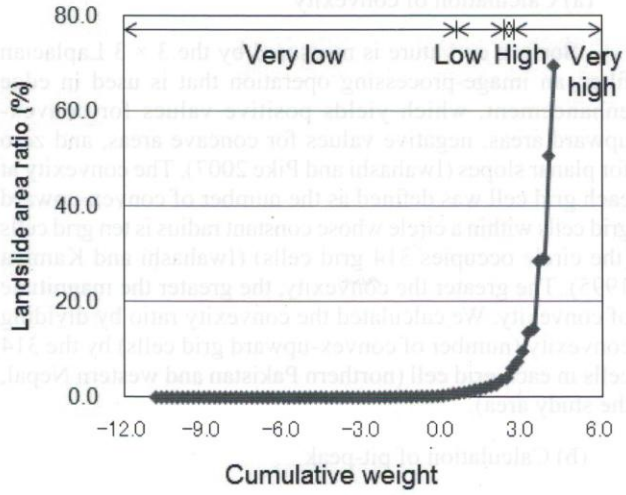


**Fig. 4: Classification of landslide susceptibility for northern Pakistan, Thresholds of cumulative weight for classification are 0.2, 2.2 and 3.0.**

## Determination of the landslide susceptibility class

Toward determining the landslide susceptibility class, we investigated "the landslide area ratio" (i.e., the ratio of landslide area in a certain class to the whole area of that class) according to the cumulative weights obtained for northern Pakistan. We classify the cumulative weights into 50 classes (interval: 0.2), then, as shown on the abscissa in Fig. 4, we calculate the landslide area ratio for each class of cumulative weight. Next, we plot the landslide area ratio according to the cumulative weight to obtain the curve shown in Fig. 4. Furthermore, we classify the curve shown Fig. 4 into four susceptibility classes using the thresholds of 0.2, 2.2, and 3.0 in cumulative weight. The corresponding landslide area ratios are 1%, 4%, and 8%, respectively (Fig. 4). The minimum and maximum landslide area ratios are 0% and 70%; therefore, the four susceptibility classes correspond to the landslide area ratio as follows: 0 - 1% in very low, 1 - 4% in low, 4 - 8% in high, 8 - 70% in very high.

Next, we apply the same thresholds of 0.2, 2.2, and 3.0 to the cumulative weight for the study area; the same four susceptibility classes as in the northern Pakistan case are also obtained for the study area. Although the earthquake-induced landslide area ratio cannot be calculated for the study area, the landslide area ratio obtained in northern Pakistan is thought to provide the best indication of landslide occurrence probability if the same magnitude of earthquake as in northern Pakistan were to occur in the study area.

## RESULTS AND DISCUSSIONS

### Mapping results of landslide susceptibility

Fig. 3c shows the susceptibility map that results from the four classifications of cumulative weight in western Nepal (Fig. 2f). The non-classified (white) areas in Fig. 3c are areas with a slope angle of less than five degrees. Fig. 3c also shows that the "very high," "high" and "low" classes exist parallel to the active fault MBF and exist on the hanging wall of the HFF. The area of the "very low" class extends far from the active faults, and the small patches of the "low" class are locally distributed within the "very low" area. Thus, the earthquake-induced landslide susceptibility is mapped in Fig. 3c. however, it is impossible to understand the susceptibility in a wide area through field survey. And susceptibility is thought to give priority to preparing for earthquake-induced landslide disaster prevention and mitigation. For example, if an important traffic network passes through a "very high" area or many residents live near such an area, the assigned slope is worth investigating in detail, so that landslide disaster preparations can be made and countermeasures taken.

Fig. 3d shows ortho-photographs (black and white, 2.5 m in resolution) taken on 30 Dec. 2006 by the Cartosat-1 satellite. "Very high" polygons are depicted in the inset in Fig. 3d. As shown in the inset image, the landslides are interpreted as pale-white denuded area in sites 1 and 2, and site 1 partially falls into the "Very high" of Fig. 3c. A landslide at site 1 may occur by heavy rain; however, an earthquake will be more likely to reactivate the landslide than the landslide at site 2, because site 2 falls into the "High" of Fig. 3c. However, the important point is that "Very high" polygons are depicted not only on the existing landslide but also on slopes where landslides were not interpreted as having occurred on the Cartosat-1 image. In preparing for earthquake-induced landslide disasters, such slopes are also worth investigating in detail.

### Map scale of landslide susceptibility and its role in preventing earthquake landslide disasters.

The map scale for landslide susceptibility is 1/25,000. If this map were depicted at the scale of 1/2,500, then a 1.2-cm cell would correspond to 30 m, and we know this scale is too coarse to apply directly to civil engineering works in the field. For example, in taking measures for disaster prevention public works in the field, the facility should be installed at the appropriate site. Because the location accuracy of a 1/25,000-scale map is lower than that of a larger-scale map, the location of the boundary between "Very high" and "High" should not be applied directly to the determination of the installation location. However, a larger scale would be redundant for an overview of the susceptibility in a wide area. The resulting susceptibility (1/25,000) is suitable for an overview of the susceptibility in a wide area. A landslide susceptibility map is used for purposes other than landslide disaster mitigation. If larger-scale susceptibility needs to be mapped, finer DEM or detailed field survey is necessary, for example, rock and sediment facies observation and crack density measurement.

Detailed field surveys are impossible in wide areas at uniform criterion. Before such surveys are done, reconnaissance investigation is always needed. In light of this, an overview of earthquake-induced landslide susceptibility mapping at 1/25,000 scale is as important as a larger-scale local map derived from detailed survey.

## CONCLUSIONS

We generated a 1/25,000-scale map of an area that has the four susceptibility classes of very low (landslide occurrence probability, 0 - 1%), low (1 - 4%), high (4 - 8%), and very high (8 - 70%). The resulting mapping scale is so small that we cannot apply it directly to civil engineering works in the field; however, because no-one can clearly focus on the sites of high probability of landslide in the field in a wide area at once, the obtained map is useful for determining what onsite locations should be surveyed. The obtained susceptibility map is a rough sketch of slopes that are candidates for measures against earthquake-induced landslide disasters.

## ACKNOWLEDEMENTS

The authors express there thanks to Associate Prof. Y. Kumahara in Gunma Univ., Japan for providing map of the active faults in western Nepal, Prof. V. Dangol, Tribhuvan University for English Proofing, Mr. S.K. Bhattachan and Mr. Raju K.C. in Kathmandu for preparation of our reconnaissance field survey in western Nepal, and Dr. J. Iwahashi in Geospatial Information Authority of Japan for help to purchase Cartosat 1 satellite image. The authors thanksful to D. Chamlagain for his helful comments and suggations to improved this manuscript.

## REFERENCES

Avouac, J. P., Pandey, M. R., Sapkota, S. N., Rajaure, S., Genrich, J., Galetzka, J., Chanard, K., Ader, T, Flouzat, M., and Bollinger, L., 2010, Where and how often shall large destructive earthquakes strike the Himalaya? Jour. Nepal Geol. Soc., v. 41, p.128.

Bilham, R., Larson, K., and Frevmueller, J., 1997, GPS measurements of present-day convergence across the Nepal Himalya. Nature, v. 386, No.6, pp. 61-64.

Chacon, J., Irigaray, C., Fernandez, T., and Hamdouni, R. E., 2006, Engineering geology maps: landslides and geographical information system. Bull. Engineering Geol. and Environment, v. 65, pp. 341-411.

Chigira, M., Wu, X., Inokuchi, T., and Wang, G., 2010, Landslides induced by the 2008 Wenchuan earthquake, Sichuan, China. Geomorphology, v. 118, pp. 225-238.

Dhakal, A. S., Amada T., and Aniya, M., 2000, Landslide hazard mapping and its evaluation using GIS: An investigation of sampling schemes for a grid-cell based quantitative method. Photogrammetric Engineering and Remote Sensing, v. 66, pp. 981-989.

Iwahashi, J. and Kamiya, I., 1995, Landform classification using digital elevation model by the skills of image processing - mainly using the digital national land information. Geoinformatics, v. 6, pp. 97-108 (in Japanese with English abstract).

Iwahashi, J. and Pike, R. J., 2007, Automated classifications of topography from DEMs by an unsupervised nested-means algorithm and a three-part geometric signature. Geomorphology, v. 86, pp. 409-440.

Iwahashi, J., Kamiya, I., and Matsuoka, M., 2010, Regression analysis of Vs30 using topographic attributes from a 50-m DEM. Geomorphology, v. 117, pp. 202-205.

Kamp, U., Growley, B. J., Khattak, G. A., and Owen, L. A., 2008, GIS-based landslide susceptibility mapping for the 2005 Kashmir earthquake region. Geomorphology, v. 101, pp. 631–642.

Kumahara, Y. and Nakata, T., 2005, Detailed mapping on active fault in developing region and its significance: A case study of Nepal. Annual Report of Research Center for Regional Geography, v. 14, pp. 113-127. Hiroshima University, Japan (in Japanese with English abstract).

Kumahara, Y. and Nakata, T., 2006, Active fault in the epicenter area of the 2005 Pakistan earthquake. Spec. Publ., No. 41, Research Center for Regional Geography, Hiroshima University, Japan (in Japanese with English abstract).

Mugnier, J.-L., Huyghe, P., Chalaron, E., and Mascle, G., 1994, Recent movements along the Main Boundary Thrust of the Himalayas: normal faulting in an overcritical thrust wedge?, Tectonophysics, v. 238, pp. 199–215.

Qi, S., Xu, Q., Lan, H., Zhang, B., and Liu, J., 2010, Spatial distribution analysis of landslides triggered by 2008.5.12 Wenchuan Earthquake, China. Engineering Geology, v. 116, pp. 95-108.

Regmi, N. R., Giardino, J. R., Vitek, J. D. and Dangol, V., 2010, Mapping landslide hazards in western Nepal: Comparing qualitative and quantitative approaches. Environmental and Engineering Geoscience, v. 16, No. 2, pp. 127-142.

Saha, A.K., Gupta, R.P., Sarkar, I., Arora, M.K., and Csaplovics, E., 2005, An approach for GIS-based statistical landslide susceptibility maps: examples and applications from a case study in Northern Spain. Natural Hazards, v.30, pp.437-449.

Sato, H.P., Sekiguchi, T., Kojiroi, R., Suzuki, Y. and Iida, M., 2005, Overlaying landslides distribution on the earthquake source, geological and topographical data: the Mid Niigata prefecture earthquake in 2004, Japan. Landslides, Vol.2, pp.143-152.

Sato, H.P., Hasegawa, H., Fujiwara, S., Tobita, M., Koarai, M., Une, H., and Iwahashi, J., 2007, Interpretation of landslide distribution triggered by the 2005 northern Pakistan earthquake using SPOT5 imagery. Landslides, v. 4, pp.113-122.

Sato, H.P. and Harp, E.L., 2009, Interpretation of earthquake-induced landslides triggered by the 12 May 2008, M7.9 Wenchuan earthquake. Landslides, v. 6, pp.153-159.

Seno, T., 2005, On the Pakistan earthquake on October 8, 2005. Journal of Geography, Vol.114, pp. 820-823. (in Japanese with English abstract)

Upreti, B.N., 1999, An over view of the stratigraphy and tectonics of the Nepal Himalaya. Jour. Asian Earth Sci., v. 17, pp. 577-606.

Van Western, C.J., 1997, Statistical landslide hazard analysis. In: Application guide, ILWIS 2.1 for Windows. ITC, Enschede, The Netherlands, pp. 73-84.

Varnes, D.J., 1984, Landslide hazard zonation: a review of principles and practice. In: *International Association of Engineering Geology Commission on Landslides and Other Mass Movements on Slopes*. UNESCO Natural Hazards Series, No. 3, 63 pp.

Yagi, H., 2003, Development of assessment method for landslide hazardness by AHP. Abstract volume of the 42nd annual meeting of the Japan Landslide Society, pp.209-212.

Yagi, H., Sato, G., Higaki, D., Yamamoto, M. and Yamasaki T., 2009, Distribution and characteristics of landslides induced by the Iwate-Miyagi Nairiku Earthquake in 2008 in Tohoku District, Northeast Japan. Landslides, v. 6, pp.335-344.

Yoshimatsu, H. and Abe, S., 2006, A review of landslide hazards in Japan and assessment of their susceptibility using an analytical hierarchic process (AHP) method. Landslides, v. 3, pp.149–158.